Springer

Journal of Mechanical Science and Technology 22 (2008) 1699~1706

Journal of Mechanical Science and Technology

www.springerlink.com/content/1738-494x
DOI 10.1007/s12206-008-0605-4

Magnetic circuit design by topology optimization for Lorentz force maximization in a microspeaker

Woochul Kim[1] and Yoon Young Kim[2,*]

[1]*CAE/TMR Group, Storage System Division, Semiconductor Business, Samsung Electronics Co., Ltd , 416, Maetan-3Dong, Yeongtong-Gu, Suwon City, Gyeonggi-Do, Republic of Korea 443-742*

[2]*National Creative Research Initiatives Center for Multiscale Design, Institute of the Advanced Machinery Design and School of Mechanical and Aerospace Engineering, Seoul National University, Slim-dong San 56-1, Kwanak-gu, Seoul, 151-742, Korea*

(Manuscript Received January 18, 2008; Revised May 25, 2008; Accepted June 8, 2008)

Abstract

Bipolar magnets are common in most magnetic circuits, but circuit efficiency can be enhanced if multipolar magnets are used instead. However, the use of multipolar magnets is rare. In this investigation, the possibility of using multipolar magnets for maximizing the Lorentz force in a microspeaker is considered. The design problem of a multipolar magnetic circuit is formulated as a topology optimization problem. The circuit design region is discretized by finite elements, and a material state among a multipolar magnet, a yoke and air for every element is so determined as to maximize a desired Lorentz force component. Numerical results show that multipolar magnetic circuits obtained by the topology optimization outperform a conventional bipolar circuit.

Keywords: Magnetic circuit; Lorentz force; Topology optimization; Microspeaker

1. Introduction

This investigation is motivated by the need to improve the efficiency of magnetic circuits in some actuating devices such as microspeakers [1, 2] and optical pickup actuators [2, 3]. In such devices, the magnetic field generated by permanent magnets and yokes is supplied to current-carrying coil for Lorentz force generation. Bipolar magnets are a typical magnetic field source but it would be possible to develop stronger magnetic field and generate larger Lorentz forces if "multipolar" magnets were used.

When the use of multipolar magnets is considered, it is more difficult to optimally distribute magnet polarities producing larger Lorentz forces under a given magnet-yoke mass constraint and a specified coil current. Because magnetic circuits can consist of multipolar magnets, yokes and an air region, standard size/shape optimization techniques cannot be used directly. Therefore, we propose to formulate the design problem as a topology optimization problem. It is a well-known advantage of the topology optimization method that it does not require any baseline design (see, e.g., [5, 6] for an overview of the method and structural applications).

Some papers [7-13] studied the topology optimization of some magnetic systems, but no investigation has been reported on multipolar magnet circuit design. Because a magnetic circuit can consist of multipolar magnets, ferromagnetic yokes and air, not only permeability (μ) but also magnetization (M) should be interpolated. The value of permeability dictates the presence of a magnet, a yoke or air at a specific location. It also determines polarization of a magnet element if a magnet turns out to be present. Therefore, design variables assigned to discretizing finite elements should be able to pick up one of three material states, i.e., a magnet, a yoke and air. To deal with multiple material states, the formulations developed

*Corresponding author. Tel.: +82 2 880 7159, Fax.: +82 2 872 5431
E-mail address: yykim@snu.ac.kr

earlier for structural [14, 15] will be modified for the present magnetic circuit design problems. Wang *et al*. [16] formulated a multi-material for magnetic problems, but the technique used in [15] will be employed here. The analysis of a magnetic circuit needed for topology optimization is carried out by a finite element method (see, e.g., [17, 18]).

Because the multipolar magnet circuit design problem is formulated as an optimization problem, an iterative gradient-based algorithm such as the method of moving asymptotes [19] can be used to update design variables or material statues of all finite elements. Design sensitivity required for the algorithm was calculated efficiently by using the adjoint variable method [20]. The optimized magnetic circuits obtained by the topology optimization formulation in this investigation were compared with a commercially available circuit for performance check.

2. Formulation for multipolar magnetic circuit design

2.1 Problem definition

Though the multipolar magnet circuit design formulated in this work is not limited to the specific problems discussed below, it will be easier to present the design issue with the following Lorentz force maximization appearing in microspeaker design.

Fig. 1(a) schematically shows a typical microspeaker used in mobile devices such as cellular phones. When alternating current flows into the coil, the Lorentz force developed in the coil actuates the diaphragm of a microspeaker. Due to axisymmetry, the predominant motion of the diaphragm along the z-axis generates an acoustic field. A ring-type coil is attached to the diaphragm. Because we are concerned with magnetic circuit design, we pay attention to the magnetic circuit illustrated in Fig. 1(b); it consists of a ring-type bipolar magnet, coil and a yoke. The magnetization vector of the magnet shown in Fig. 1(b) is $+M\mathbf{e}_z$ where M is the magnitude of magnetization and $\mathbf{e}_z$ is the unit vector in the direction of z. A magnetic flux distribution by the magnetic circuit in Fig. 1(b) is shown in Fig. 1(c). ANSYS [21] was used to obtain the results shown in Fig. 1(c). The parameter r_c in Fig. 1(b) denotes the location of the center of the ring coil to r direction.

When the generated magnetic flux density by a magnet is denoted by **B**, the Lorentz force **F** developed in the coil can be written as

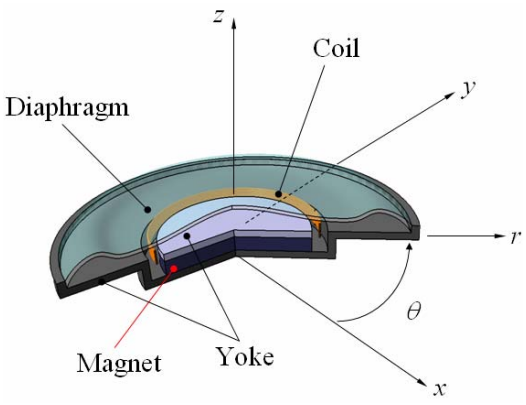

(a)

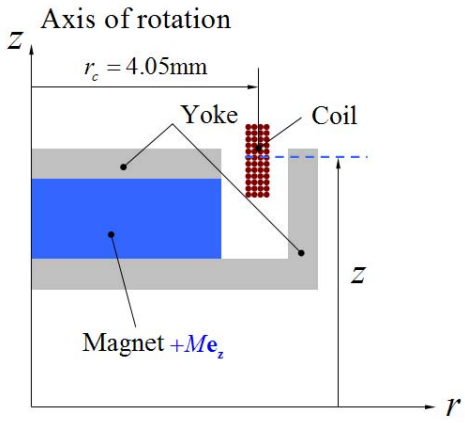

(b)

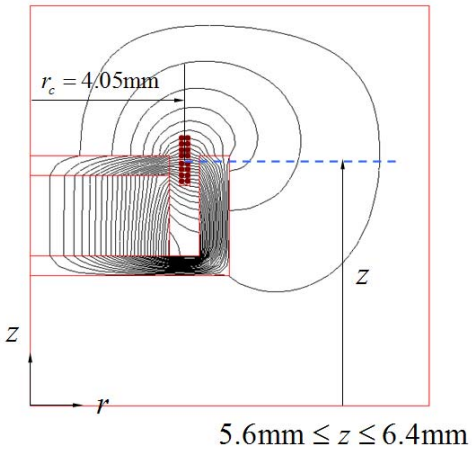

(c)

Fig. 1. (a) Schematic illustration of a nominal microspeaker, (b) two-dimensional axisymmetric model, and (c) magnetic flux distribution.

$$\mathbf{F} = I\oint_C \mathbf{dl}\times\mathbf{B} = \oint_V \mathbf{J}dV\times\mathbf{B} \quad (1)$$

where I and $\mathbf{dl}$ denote the current flowing into the coil and an infinitesimal line element of the coil. The symbol **J** expresses volume current density, current flowing through a unit area normal to the current flow direction. As Eq. (1) shows, the magnitude of the Lorentz force is proportional to the magnitude of the magnetic flux density. Thus, a magnetic circuit generating larger flux density produces a larger Lorentz force and a higher sound pressure level. To find an optimal magnetic circuit, the region currently occupied by the ring-type bipolar magnet and the yokes is chosen to be the magnetic circuit design domain. An optimal multipolar magnetic circuit configuration maximizing the Lorentz force f_z in the axial direction z will be configured by a topology optimization, which is given in the next section.

2.2 Design setup as a topology optimization problem

The design objective is to find an optimal magnetic circuit maximizing the Lorentz force in a specific direction while the possibility of multipolarities of a magnet is taken into account. Because the polarization direction of the ring-type magnet in a microspeaker is the z direction as shown in Fig. 1(b), only the polarizations along $\pm z$ will be considered in this investigation. Though the topology optimization formulation set up here can be used for more general magnetic circuit design problems, the formulation will be specifically suited for the design of a multipolar magnetic circuit of a microspeaker.

To find a multipolar magnetic circuit maximizing the Lorentz force f_z in the z direction, the region occupied by a magnet and yokes in Fig. 1(b) is selected as the design domain for topology optimization; see Fig. 2. Because of the axisymmetric characteristics of the design problem, the region is discretized by axisymmetric finite elements. Each finite element in Fig. 3 denotes an axisymmetric finite element.

For the eth finite element, N_m design variables $(\gamma_1^e, \gamma_2^e, \cdots, \gamma_{N_m}^e)$ are defined. For the microspeaker design problem depicted in Fig. 3, N_m =2 if only bipolar magnets are considered: a magnet state with $+M\mathbf{e}_z$, a yoke state, and an air state. (Note that an element is filled with air if no magnet or yoke appears in it.) However, if multipolar magnets are considered, there are four possible states such as two magnet

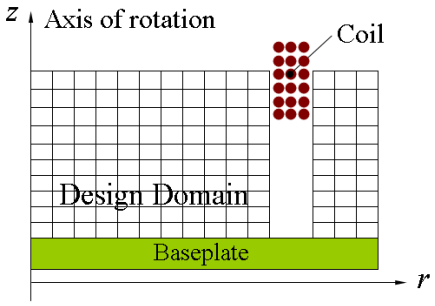

Fig. 2. Design domain for the optimization of a multipolar magnetic circuit of a microspeaker.

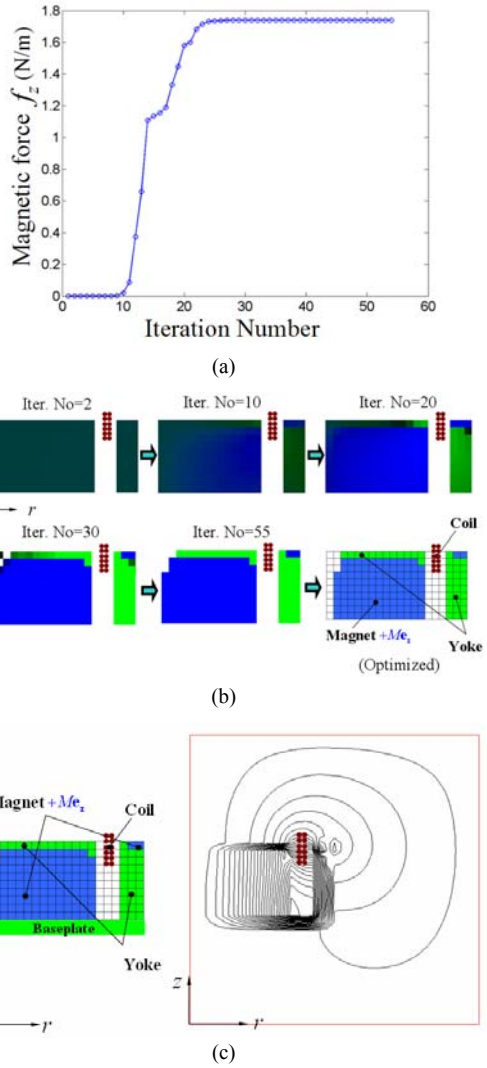

Fig. 3. Optimized result for CASE A (bipolar magnetic circuit optimization). (a) Optimization history, (b) intermediate and final circuit configurations at some optimization iteration steps, (c) magnetic flux distribution.

states with $\pm M\mathbf{e}_z$, a yoke state and an air state. In this case, therefore, N_m =3.

To solve the multipolar design problem in the topology optimization setting, the side constraints must be assigned to the design variables:

$$10^{-4} = \gamma_{\min} \le \gamma_i^e \le 1 \quad \text{for} \quad i = 1,2,\cdots,N_m, \quad e = 1,2,\cdots,N \tag{2}$$

where $\gamma_i^e = \gamma_{\min}$ and $\gamma_i^e = 1$ stand for the absence and the presence of the i^{th} material state, respectively. The total number of discretizing finite elements is denoted by N. To ensure that either $\gamma_i^e = \gamma_{\min}$ or $\gamma_i^e = 1$ is reached without ambiguous intermediate values in the final optimization iteration step, a penalization scheme must be introduced to interpolate two material parameters μ and M. Therefore, the penalization scheme developed in [14, 15] may be converted to

$$\frac{1}{\mu^e(\boldsymbol{\gamma}^e)} = \frac{1}{\mu_0} + \sum_{i=1}^{N_m} \underbrace{\left[(\gamma_i^e)^p \prod_{j=1}^{N_m} \left[1 - (\gamma_{j\neq i}^e)^q \right] \right]}_{\phi_i^e(\boldsymbol{\gamma}^e)} \left(\frac{1}{\bar{\mu}_i} - \frac{1}{\mu_0} \right) \quad (e = 1,2,\cdots,N) \tag{3}$$

$$M^e(\boldsymbol{\gamma}^e) = \sum_{i=1}^{N_m} \underbrace{\left[(\gamma_i^e)^p \prod_{j=1}^{N_m} \left[1 - (\gamma_{j\neq i}^e)^q \right] \right]}_{\phi_i^e(\boldsymbol{\gamma}^e)} \bar{M}_i \quad (e = 1,2,\cdots,N) \tag{4}$$

where Π denotes a multiplication operator. In Eqs. (3) and (4), μ_0 is free-space permeability. The permeability and magnetization of the i^{th} material state are denoted by $\bar{\mu}_i$ and $\bar{M}_i$, respectively. The symbol ϕ_i^e implies the participation factor of the i^{th} material in the permeability μ^e and M^e of the e^{th} element. The superscripts p and q are penalty exponents.

Note that for N_m =3, we have the following relations:

Material 1 (ferromagnetic yoke): $\bar{\mu}_1 = \mu_F$ and $\bar{M}_1 = 0$

Material 2 (permanent magnet with $\mathbf{M} = M_p\mathbf{e}_z$): $\bar{\mu}_2 = \mu_M$ and $\bar{M}_2 = +M_P$

Material 3 (permanent magnet with $\mathbf{M} = -M_p\mathbf{e}_z$): $\bar{\mu}_3 = \mu_M$ and $\bar{M}_3 = -M_P$

where μ_F and μ_M denote the permeability of a yoke and permanent magnet material and M_P, the amount of magnetization of a permanent magnet. In this case, the combinations of design variables having upper or lower limits represent either one of the materials:

$(\gamma_1^e = 1, \gamma_2^e = 0, \gamma_3^e = 0) \rightarrow$ Material 1
$(\gamma_1^e = 0, \gamma_2^e = 1, \gamma_3^e = 0) \rightarrow$ Material 2
$(\gamma_1^e = 0, \gamma_2^e = 0, \gamma_3^e = 1) \rightarrow$ Material 3
$(\gamma_1^e = 0, \gamma_2^e = 0, \gamma_3^e = 0) \rightarrow$ Air

To find an optimal multipolar magnetic circuit by topology optimization, the following problem will be solved:

$$\underset{\boldsymbol{\gamma}}{\text{Maximize}} \; f_z|_{\text{Coil}} = \sum_{j=1}^{N_c} [{}^jJ_\theta \times {}^jB_r(\boldsymbol{\gamma})] = \underset{1\times N_c}{[\mathbf{J}_\theta]} \underset{N_c\times 1}{[\mathbf{B}_r(\boldsymbol{\gamma})]} \tag{5a}$$

with

$$m_i = \sum_{e=1}^{N} \gamma_i^e V_e \le \bar{m}_i \quad (i = 1,\cdots,N_m) \tag{5b}$$

$$m_{total} = \sum_{e=1}^{N_m} m_i \le \bar{m}_{total} \tag{5c}$$

$$\boldsymbol{\gamma}^e = \{\gamma_1^e, \gamma_2^e \cdots, \gamma_{N_m}^e\}^T \tag{5d}$$

$$\boldsymbol{\gamma} = \{\boldsymbol{\gamma}^1, \boldsymbol{\gamma}^2 \cdots, \boldsymbol{\gamma}^N\}^T \tag{5e}$$

In Eq. (5a), $f_z|_{\text{Coil}}$ is the total Lorentz force generated by the coil (see Fig. 3). The symbol j in Eq. (3) denotes the j^{th} segment of the coil discretized along the z-axis at r_c and N_c, the number of segments for force calculation. For the problem in consideration, force calculation points are chosen at r_c = 4.05 mm along the z-axis (5.6 mm $\le z \le$ 6.4 mm). The value of N_c =10 is used. The coil shape and location are assumed to remain unchanged during optimization. Referring to Eq. (1), two Lorentz force components, f_r and f_z, can be developed because the current density has only the component in the θ direction, but only the f_z component is maximized because it is the driving force of the diaphragm. Eqs. (5b) and (5c) correspond to mass constraints. Eq. (5b) states that the mass of the i^{th} material m_i cannot exceed the upper bound value $\bar{m}_i$. At the same time, the total mass m_{total} cannot exceed the prescribed total mass $\bar{m}_{total}$ by Eq. (5c).

To solve Eq. (5), the radial component B_r must be calculated for any magnetic circuit configuration appearing during topology optimization. To this end,

one may use the following weak form to solve a linear axisymmetric electromagnetic problem [18]:

$$\min \chi(A_\theta^P) = \int_S \frac{1}{2}\left\{\frac{1}{\mu_r}\left(\frac{\partial A_\theta^P}{\partial z}\right)^2 + \frac{1}{\mu_z}\left(\frac{A_\theta^P}{r} + \frac{\partial A_\theta^P}{\partial r}\right)^2\right\} 2\pi r dr dz - \int_S \left(\frac{\partial M_r}{\partial z} - \frac{\partial M_z}{\partial r}\right) A_\theta^P 2\pi r dr dz \tag{6}$$

with

$$B_r = -\frac{\partial A_\theta^P}{\partial z},\ B_z = \frac{1}{r}\frac{\partial}{\partial r}\left(rA_\theta^P\right) \tag{7}$$

In Eqs. (6) and (7), A_θ^P is the θ component of a vector magnetic potential $\mathbf{A}^P$, M_r and M_z denote the r and z components of magnetization. Following a standard procedure for finite element discretization [17, 18], a matrix equation corresponding to Eqs. (6) and (7) can be obtained. The results can be written in symbolic form as:

$$\mathbf{K}_\mathrm{A}\mathbf{A} = \mathbf{F}_\mathrm{A} \tag{8}$$

$$B_r = -\frac{\partial \mathbf{N}^T}{\partial z}\mathbf{A} \tag{9}$$

where $\mathbf{N}$ is the interpolation function (bilinear interpolation functions were used in this work) and the symbol T stands for matrix transpose. $\mathbf{K}_\mathrm{A}$ and $\mathbf{F}_\mathrm{A}$ denote the system stiffness matrix and the system load vector constructed from the assembly of element-level stiffness matrices $\mathbf{k}^e$ and load vectors $\mathbf{f}^e$ as

$$\mathbf{K}_\mathrm{A} = \sum_{e=1}^{N} \mathbf{k}^e(\boldsymbol{\gamma}^e)\ ;\ \ \mathbf{F}_\mathrm{A} = \sum_{e=1}^{N} \mathbf{f}^e(\boldsymbol{\gamma}^e) \tag{10a,b}$$

where $\sum$ is an assembly operator for finite elements. A selection of one material state among N_m materials is considered for every element, and the material parameter interpolation scheme of Eqs. (3) and (4) must be used for topology optimization. Therefore, one may replace Eqs. (3) and (4) with the following element-level matrix and load vector interpolation [15]:

$$\mathbf{k}^e(\boldsymbol{\gamma}^e) = \sum_{i=1}^{N_m} \phi_i^e(\boldsymbol{\gamma}^e)\bar{\mathbf{k}}_i^e = \sum_{i=1}^{N_m} \underbrace{\left[(\gamma_i^e)^p \prod_{\substack{j=1 \\ j\neq i}}^{N_m}\left[1-(\gamma_j^e)^q\right]\right]}_{\phi_i^e(\boldsymbol{\gamma}^e)} \bar{\mathbf{k}}_i^e \tag{11}$$

$$\mathbf{f}^e(\boldsymbol{\gamma}^e) = \sum_{i=1}^{N_m} \phi_i^e(\boldsymbol{\gamma}^e)\bar{\mathbf{f}}_i^e = \sum_{i=1}^{N_m} \underbrace{\left[(\gamma_i^e)^p \prod_{\substack{j=1 \\ j\neq i}}^{N_m}\left[1-(\gamma_j^e)^q\right]\right]}_{\phi_i^e(\boldsymbol{\gamma}^e)} \bar{\mathbf{f}}_i^e \tag{12}$$

In Eqs. (11) and (12), $\bar{\mathbf{k}}_i^e$ and $\bar{\mathbf{f}}_i^e$ are design-variable independent quantities. When four-node bilinear finite elements are used, the components of $\bar{\mathbf{k}}_i^e$ and $\bar{\mathbf{f}}_i^e$ are given as [18]

$$\bar{k}_{ab}^e = \int_{S^e} 2\pi\left[\frac{1}{\mu}\left(\frac{N_b}{r} + \frac{\partial N_b}{\partial r}\right)\left(\frac{N_a}{r} + \frac{\partial N_a}{\partial r}\right) + \frac{1}{\mu}\frac{\partial N_a}{\partial z}\frac{\partial N_b}{\partial z}\right] r dr dz \tag{13a}$$

$$\bar{f}_a^e = \int_{S^e} 2\pi\left(\frac{\partial M_r}{\partial z} - \frac{\partial M_z}{\partial r}\right) N_a r dr dz \quad (a,b = 1,2,3,4) \tag{13b}$$

where N_a denotes the interpolation function associated with element node a.

So far, the procedure to compute $B_r(\boldsymbol{\gamma})$ and thus $f_z|_\mathrm{Coil}(\boldsymbol{\gamma})$ in Eq. (5) has been explained. To solve Eq. (5) by an iterative numerical procedure, the method of moving asymptotes (MMA) [19], an efficient gradient optimizer, will be employed. To use MMA, the sensitivity of $f_z|_\mathrm{Coil}(\boldsymbol{\gamma})$ with respect to $\boldsymbol{\gamma}^e$ must be calculated. The explicit sensitivity can be obtained by a standard procedure, but it will be given for the sake of completeness:

$$\begin{aligned}\frac{d}{d\boldsymbol{\gamma}} f_z|_\mathrm{Coil}(\boldsymbol{\gamma}) &= \left(\frac{\partial}{\partial \mathbf{A}} f_z|_\mathrm{Coil}(\boldsymbol{\gamma})\right)^T \frac{\partial \mathbf{A}}{\partial \boldsymbol{\gamma}} \\ &= \left(-\mathbf{J}_\theta \frac{\partial \mathbf{N}}{\partial z}\right)^T \mathbf{K}_\mathrm{A}^{-1}\left(-\frac{\partial \mathbf{K}_\mathrm{A}}{\partial \boldsymbol{\gamma}}\mathbf{A} + \frac{\partial \mathbf{F}_\mathrm{A}}{\partial \boldsymbol{\gamma}}\right)\end{aligned} \tag{14}$$

To avoid the explicit matrix inversion of $\mathbf{K}_\mathrm{A}^{-1}$, it is convenient to introduce an adjoint variable $\boldsymbol{\lambda}$ satisfying the following Eq. (see, e.g. [20]):

$$\mathbf{K}_\mathrm{A}\boldsymbol{\lambda} = \left(-\mathbf{J}_\theta \frac{\partial \mathbf{N}}{\partial z}\right)^T \tag{15}$$

Substituting Eq. (15) into Eq. (14) yields

$$\begin{aligned}\frac{d}{d\boldsymbol{\gamma}} f_z|_\mathrm{Coil}(\boldsymbol{\gamma}) &= \left(\frac{\partial}{\partial \mathbf{A}} f_z|_\mathrm{Coil}(\boldsymbol{\gamma})\right)^T \frac{\partial \mathbf{A}}{\partial \boldsymbol{\gamma}} \\ &= \boldsymbol{\lambda}^T\left(-\frac{\partial \mathbf{K}_\mathrm{A}}{\partial \boldsymbol{\gamma}}\mathbf{A} + \frac{\partial \mathbf{F}_\mathrm{A}}{\partial \boldsymbol{\gamma}}\right)\end{aligned} \tag{16}$$

In Eq. (17), $\partial \mathbf{K}_{\mathrm{A}} / \partial \gamma_k^e$ and $\partial \mathbf{F}_{\mathrm{A}} / \partial \gamma_k^e$ are expressed as

$$\frac{\partial \mathbf{K}_{\mathrm{A}}}{\partial \gamma_k^e} = p\left(\gamma_k^e\right)^{p-1} \prod_{\substack{j=1 \\ j\neq k}}^{N_m} \left[1-(\gamma_j^e)^q\right] \bar{\mathbf{k}}_k^e - q(\gamma_k^e)^{q-1} \sum_{\substack{i=1 \\ i\neq k}}^{N_m} \left[(\gamma_i^e)^p \prod_{\substack{j=1 \\ j\neq i, j\neq k}}^{N_m} \left[1-(\gamma_j^e)^q\right] \right] \bar{\mathbf{k}}_i^e \quad (17)$$

$$= \frac{p}{\gamma_k^e} \phi_k^e(\boldsymbol{\gamma}^e) \bar{\mathbf{k}}_k^e - \frac{q\left(\gamma_k^e\right)^{q-1}}{1-\left(\gamma_k^e\right)^q} \sum_{\substack{i=1 \\ i\neq k}}^{N_m} \phi_i^e(\boldsymbol{\gamma}^e) \bar{\mathbf{k}}_i^e$$

$$\frac{\partial \mathbf{F}_{\mathrm{A}}}{\partial \gamma_k^e} = p\left(\gamma_k^e\right)^{p-1} \prod_{\substack{j=1 \\ j\neq k}}^{N_m} \left[1-(\gamma_j^e)^q\right] \bar{\mathbf{f}}_i^e - q(\gamma_k^e)^{q-1} \sum_{\substack{i=1 \\ i\neq k}}^{N_m} \left[(\gamma_i^e)^p \prod_{\substack{j=1 \\ j\neq i, j\neq k}}^{N_m} \left[1-(\gamma_j^e)^q\right] \right] \bar{\mathbf{f}}_i^e \quad (18)$$

$$= \frac{p}{\gamma_k^e} \phi_k^e(\boldsymbol{\gamma}^e) \bar{\mathbf{f}}_i^e - \frac{q\left(\gamma_k^e\right)^{q-1}}{1-\left(\gamma_k^e\right)^q} \sum_{\substack{i=1 \\ i\neq k}}^{N_m} \phi_i^e(\boldsymbol{\gamma}^e) \bar{\mathbf{f}}_i^e$$

3. Numerical results and discussions

Though multipolar magnetic circuit design is the main objective, it would be interesting to compare an optimized "bipolar" magnetic circuit and an optimized "multipolar" magnetic circuit. For numerical analysis, the following data were used:

$\mu_0 = 4\pi \times 10^{-7}$ H/m ,

$\mu_Y = 1000\mu_0$ for yoke

$\mu_M = 1.02\mu_0$, $B_r = 1.17$ T , $M_p = 1190400$ A/m for Nd-Fe-B type permanent magnet

Case A: Bipolar magnetic circuit optimization

First, we consider the design optimization of a bipolar magnetic circuit. This means that magnet material having $+M_p\mathbf{e}_z$, yoke material or air can be assigned to each of the finite elements discretizing the design domain. Therefore, $N_m = 2$ in this case. The values of p=3 and q=2 were selected for Eqs. (11) and (12). The mass constraints on the magnet and yoke are 70% and 30% of the total mass of the design domain.

The variation of the objective function $f_z|_{\mathrm{Coil}}$ during the topology optimization is plotted in Fig. 3(a). The initial values of design variables were γ_1^e=0.6 and γ_2^e=0.6 ($e = 1, \cdots, N$). Fig. 3(b) shows magnetic circuit configurations appearing during optimization iterations. Fig. 3(c) shows the optimized magnetic circuit installed to a baseplate and the flux distribution analyzed by ANSYS for the optimized circuit. Unlike in the nominal circuit in Fig. 1(a), two sets of magnets appear in the magnetic circuit. Furthermore, no material is present near r=0. The actual Lorentz forces by the optimized magnetic configuration in Fig. 4 are compared with those by the nominal, or conventional, magnetic configuration shown in Fig. 1. Note again that the magnetic force is calculated at $r_c = 4.05$ mm along the z-axis ($5.6 \text{ mm} \le z \le 6.4$ mm). For all coil locations, the optimized circuit outperforms the nominal circuit.

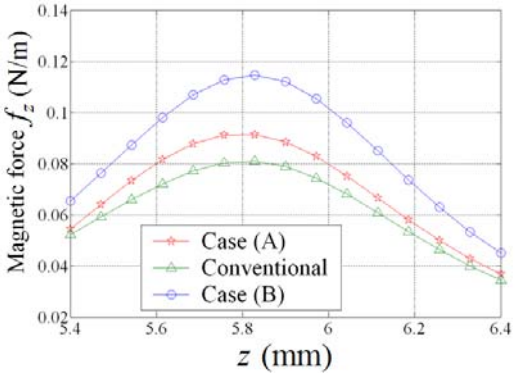

Fig. 4. Comparison of the axial Lorentz forces by three magnetic circuits for varying coil center locations.

Case B: Multipolar magnetic circuit optimization

In this case, magnets having either $+M_p\mathbf{e}_z$ or $-M_p\mathbf{e}_z$ can appear in addition to yokes or air. Therefore, $N_m = 3$. The mass constraint on the yoke is 20 % of the total mass of the design domain and the constraints on the magnets having $+M_p\mathbf{e}_z$ and $-M_p\mathbf{e}_z$ are 65% and 15%, respectively. The optimization history and the circuit configuration variation during iterations are shown in Fig. 5(a) and (b), respectively. The initial values of design variables were γ_1^e=0.25 and γ_2^e=0.25 ($e = 1, \cdots, N$). In comparison with the optimized bipolar magnetic circuit shown in Fig. 4, not only a magnet with $+M_p\mathbf{e}_z$ but also a magnet with $-M_p\mathbf{e}_z$ appeared in the circuit. In addition, the yoke location of Case B is quite different from that of Case A: compare Fig. 3(c) and Fig. 5(c). The flux line passing through the coil is also plotted in Fig. 5(c).

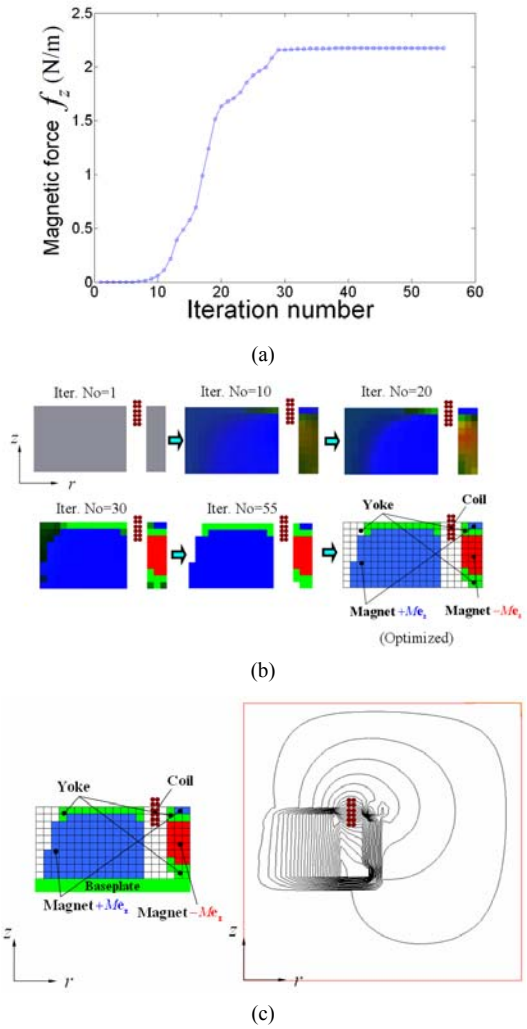

Fig. 5. Optimized result for CASE B (multipolar magnetic circuit optimization). (a) Optimization history, (b) intermediate and final circuit configurations at some optimization iteration steps, (c) magnetic flux distribution.

Finally, the Lorentz forces developed in the coil by the optimized multipolar magnetic circuit are plotted in Fig. 4. It shows that the optimized multipolar circuit performs best among three configurations considered. The reason for larger magnetic forces by the optimized multipolar magnet is that two oppositely magnetized magnets can generate larger magnetic flux compared to other configurations. One can compare the flux lines in Fig. 1(c), Fig. 3(c) and Fig. 5(c). In addition, yokes located between the oppositely magnetized magnets help concentrate the magnetic flux further onto the coil.

In comparison with the nominal magnetic circuit, the optimized circuits in Case A and Case B increased the axial Lorentz force considerably as confirmed by Fig. 4. No additional mass was used to solve Cases A and B. The design was performed for the same current input and coil configuration. From the practical point of view, the complexity of the magnetic circuit configurations in Fig. 3(c) and Fig. 5(c) may increase fabrication cost. However, the superior performance of the proposed circuits could offset the cost increase.

4. Conclusions

Although multipolar magnetic circuits can improve circuit efficiency, they are rarely used in practice. In this work, the idea of using a multipolar magnetic circuit to maximize the Lorentz force was tested in a microspeaker. Because the circuit is allowed to consist of magnets of different polarities, yokes and air, it is difficult to find an optimal circuit configuration by trial and error. To overcome this difficulty, the design problem was set up as a topology optimization of a magnetic system, and a formulation suitable to deal with multipolar magnets was presented. The optimized multipolar magnetic circuit was shown to yield about 28% larger Lorentz forces than a conventional, un-optimized bipolar magnetic circuit. The design optimization method developed in this work can be a powerful tool in designing more general multipolar magnetic configurations.

Acknowledgments

This research was supported by the National Creative Research Initiatives Program (Korea Science and Technology Foundation grant No. 2007-019) contracted through the Institute of Advanced Machinery and Design at Seoul National University.

References

[1] G. Y. Hwang, K. T. Kim, S. U. Chung, S. M. Hwang, I. C. Hwang and B. S. Kang, Analysis of a dynamic speaker in mobile phones by considering mechanical, electrical, and magnetic coupling effects, *J. of Appl. Phys*. 91 (2002) 6979-6981.

[2] S.-M. Hwang, G.-Y. Hwang, S.-H. Park, B.-S. Kang and D.-W. Lee, Performance design of a dynamic receiver for personal communication devices using finite element method, *Journal of Magnetism and Magnetic Materials* 226 (2001) 1245-1236.

[3] S.-N. Hong, I.-H. Choi, Y.-J. Kim, M.-S. Suk and J.-Y. Kim, Force characteristics of slim pick actuator to improve actuating performances, *Jpn. J. Appl. Phys.* 40 (2001) 1771-1774.

[4] W. Kim, J. E. Kim and Y. Y. Kim, Coil configuration design for the Lorentz force maximization by the topology optimization method: applications to optical pickup coil design, *Sensors and Actuators A* 121 (2005) 221-229.

[5] M. P. Bendsøe and O. Sigmund, Topology Optimization Theory, Methods and Applications, Springer-Verlag: New York, (2003).

[6] G. H. Yoon and Y. Y. Kim, The role of S-shaped mapping functions in the SIMP approach for topology optimization, *KSME Int. J*. 15 (2003) 1496-1506.

[7] L. Yin and G. K. Ananthasuresh, A novel topology design scheme for the multi-physics problems of electro-thermally actuated compliant micromechanisms, *Sensors and Actuators A* 97-98 (2002) 599-609.

[8] J. Simkin and C. W. Trobridge, Optimization problem in electromagnetics, *IEEE Trans. Mag.* 27 (27) (1991) 4016-4019.

[9] W. Kim and Y. Y. Kim, Design of a bias magnetic system of a magnetostrictive sensor for flexural wave measurement, *IEEE Trans. Mag*. 40 (5) (2004) 3331-3338.

[10] S. H. Cho, Y. Kim and Y. Y. Kim, The optimal design and experimental verification of the bias magnet configuration of a Magnetostrictive Sensor for bending wave measurement, *Sensors and Actuators A*. 107 (2003) 225-232.

[11] C. I. Park, W. Kim, S. H. Cho and Y. Y. Kim, Surface-detached v-shaped yoke of obliquely-bonded magnetostrictive strips for high transduction of ultrasonic tortional waves, *Appl. Phys. Lett*. 87 (2005) 224105.

[12] Dreck. N. Dyck and David A. Lowther, Automated design of magnetic devices by optimizing material distribution, *IEEE Trans. Mag*. 32 (3) (1996) 1188-1192.

[13] I. K. Kim, W. Kim and Y. Y. Kim, Magnetostrictive grating with an optimal yoke for generating high-output frequency-tuned SH Waves in a plate, *Sensors and Actuators A*. 137 (2007) 141-146.

[14] J. Stegmann and E. Lund, Discrete material optimization of general composite shell structures, *International Journal for Numerical Methods in Engineering*, 32 (2005) 2009-2027.

[15] G. H Yoon, Y. K. Park and Y. Y. Kim, Element Stacking Method for Topology Optimization with Material-dependent Boundary and Loading, *Journal of Materials and Mechanics of Structures* 2 (5) (2007) 132-146.

[16] S. Wang, S. Park and J. Kang, Multi-domain Topology Optimization of Electromagnetic Systems, *COMPEL* 23 (4) (2004) 1036-1044.

[17] S. J. Salon, Finite Element Analysis of Electrical Machines, Kluwer Academic Publishers, New York, (1995).

[18] J. Jin, The Finite Element Method in Electromagnetics, John Wiley & Sons, Inc., New York, (2001).

[19] K. Svanberg, The method of Moving Asymptotes-a new method for structural optimization, *Int. J. Numer. Mech.* 24 (1987) 359-373.

[20] E. J. Haug, K. K. Choi and V. Komkov, Design Sensitivity Analysis of Structural Systems, Academic Press, New York, (1986).

[21] ANSYS, User's Manuals, 2003.